OPEN ACCESS
IOP Publishing
Journal of Physics D: Applied Physics
J. Phys. D: Appl. Phys. 56 (2023) 074003 (10pp)
https://doi.org/10.1088/1361-6463/acaf0b

Gain measurements on VCSEL material using segmented contact technique

C Hentschel[1,*], C P Allford[1], S-J Gillgrass[1], J Travers-Nabialek[1], R Forrest[1], J Baker[1], J Meiklejohn[1], D Powell[2], W Meredith[2], M Haji[3], J I Davies[4], S Shutts[1] and P M Smowton[1]

[1] EPSRC Future Compound Semiconductor Manufacturing Hub, School of Physics and Astronomy, Cardiff University, Cardiff, United Kingdom
[2] Compound Semiconductor Centre, Cardiff, United Kingdom
[3] National Physical Laboratory, Teddington, United Kingdom
[4] IQE plc, Cardiff, United Kingdom

E-mail: hentschelct@cardiff.ac.uk

Received 30 June 2022, revised 19 December 2022
Accepted for publication 29 December 2022
Published 31 January 2023

Abstract

We report direct measurements of the optical gain on vertical-cavity surface-emitting laser (VCSEL) material using a stripe-length method featuring segmented contacts. We utilise the similarity of the in-plane transverse electric (TE) polarised matrix element and that of the VCSEL lasing mode and a simple method to reduce round trip effects. The confinement factor is determined from cold-cavity simulations of the in-plane TE polarised slab waveguide mode and used to convert the measured in-plane modal gain into the vertical-cavity modal gain, as required for the VCSEL structure. This gives a threshold material gain of 1440 ± 140 cm^{-1} at 30 °C for this structure. A comparison with the threshold material gain values determined from the lasing condition, where internal optical losses due to doping induced absorption is included using parameters taken from the literature, indicates the presence of an additional source of optical loss in the experiment which increases the threshold material gain by $\sim$450 cm^{-1}. A best fit is obtained by increasing the optical loss in the n-DBR (distributed Bragg reflectors) layers to 40 cm^{-1}, which is consistent with previous work on additional scattering losses due to interface roughening in the n-DBR layers. To further demonstrate the utility of this method for rapid optimisation, the gain-peak wavelength is measured directly, and its temperature dependence is compared to the lasing wavelength.

Keywords: VCSEL, optical gain, segmented contact, stripe-length

(Some figures may appear in colour only in the online journal)

1. Introduction

A large growth in the vertical-cavity surface-emitting laser (VCSEL) [1] market is expected to continue over the next few years, particularly in sensing applications, such as face and gesture recognition [2, 3]. The emergence of specialised miniature atomic sensors requiring VCSELs that meet stringent requirements [4–7] has further increased the need for the testing and verification of VCSEL epitaxial structures to ensure desired specifications are met. This can be achieved by a combination of growth calibrations such as room temperature photoluminescence and cavity resonance reflectance measurements plus fabrication of full VCSEL structures, to give laser output characteristics tested at the wafer-level. However, making informed decisions on appropriate changes to the epitaxial

[*] Author to whom any correspondence should be addressed.

Original content from this work may be used under the terms of the Creative Commons Attribution 4.0 licence. Any further distribution of this work must maintain attribution to the author(s) and the title of the work, journal citation and DOI.

Table 1. Comparison of this work with previous work on the characterisation of active layers in VCSEL material.

Authors	Publication Year	VCSEL Gain Measurement Technique	Result
Geels *et al* [17]	1991	External efficiency of in-plane laser	Gain value at gain peak wavelength
Kuksenkov *et al* [10]	1995	External efficiency of VCSEL	Gain value at cavity wavelength
Thibeault *et al* [11]	1995	External efficiency of VCSEL	Gain value at cavity wavelength
Kajita *et al* [18]	1995	In-plane Hakki–Paoli	Gain spectrum
Babic *et al* [12]	1997	External efficiency of VCSEL	Gain value at cavity wavelength
Ghosh *et al* [19]	2000	Electro-luminescence (EL)	EL spectrum
Hofmann *et al* [13]	2002	In-plane transmission[a]	Gain spectrum[a]
Lu *et al* [9]	2008	Vertical Hakki–Paoli	Gain spectrum
Ikyo *et al* [14]	2016	In-plane laser wavelength[a]	Gain-peak wavelength[a]
This Work		In-Plane segmented contact method	Gain spectrum

[a] Measurement performed on reference sample with nominally identical active layers.

structure to optimise device performance is challenging. The threshold gain requirement arising from the structure must be well characterised and sources of optical loss identified. Furthermore, to ensure efficient operation, with low threshold current, the gain-peak should coincide with the cavity resonance; this is complicated since each of these parameters has a different temperature dependence, with typical thermal tuning coefficients of 0.06 nm K^{-1} and 0.3 nm K^{-1} for the cavity resonance and the gain-peak wavelength respectively [5]. A full understanding of how the optical gain spectrum varies with temperature and current density would enable more rapid optimization at lower cost.

Compared to their edge emitting counterparts, gain characterisation of the active layers within VCSEL structures is not as straightforward. The highly reflective distributed Bragg reflectors (DBR), which form the vertical cavity, make single pass gain measurement techniques difficult to apply in the vertical direction. While the Hakki–Paoli technique [8] has been applied in the vertical direction on a 24.5-λ cavity VCSEL [9], this is not possible with few-λ cavity VCSEL structures due to their large free spectral range. The gain-current relation has also been determined from measurements of the external quantum efficiency and threshold current, with losses varied by changing the feedback from an external mirror [10], or by changing the internal optical loss by fabricating different area devices [11, 12]. Methods using the external efficiency on VCSEL devices are compatible with on-wafer testing. However, only the value at the cavity resonance wavelength can be determined, and often requires estimating (or additional measurements to determine) parameters such as the injection efficiency to accurately determine the losses from the external efficiency or calculating the mirror loss due to the DBR and external mirror. Where losses are varied by changing the area, the injection efficiency may also differ between devices.

Alternatively, the gain can be measured by looking at the in-plane propagation of light. Test wafers can be grown with a nominally identical active region and without the Bragg reflectors [13, 14], but there may be differences in current injection and is less useful than testing on the very same structure and wafer used for fully operational VCSEL devices.

Although the VCSEL structure is designed for vertical emission, light can propagate in the plane of the VCSEL material [15–19]. In many cases, the in-plane mode can propagate with low optical loss, as the separate confinement heterostructure (SCH) effectively forms a multi-layer slab waveguide [16, 17]. It is therefore possible to apply in-plane gain measurement techniques directly on VCSEL material. Previous reports include the fabrication of different length stripe lasers, and the peak-gain current density curve was obtained from measurements of the in-plane external quantum efficiency and threshold current [17]. This is a relatively simple measurement and it is possible to determine the injection efficiency by fabricating different length stripe lasers. However, gain values are limited to the in-plane lasing wavelength. The in-plane Hakki–Paoli method has also been applied on VCSEL material, although carrier pinning limited the measured gain spectra to subthreshold current densities [18].

Here, we investigate the optical gain characteristics of VCSEL material using a stripe-length method [20] to measure the in-plane modal-gain as a function of carrier injection for a range of operating temperatures; an approach which, to our knowledge, has not previously been used on VCSEL material. Table 1 compares this work with previous work on the characterisation of active layers in VCSEL material. In this work, we have applied the segmented contact method on VCSEL material, and suppressed lasing using a simple technique, so that the optical gain can be characterised at current densities close to where a VCSEL operates. We have measured the gain as a function of temperature and compared this to the device operating point.

For both the vertical lasing mode of the VCSEL, and the transverse electric (TE) polarised in-plane mode, the electric field is polarised in the plane of the quantum wells (QW). The photon momentum should be small compared to the crystal momentum, so despite the propagation direction being orthogonal, the dipole matrix element which determines the optical gain for each mode will effectively be identical for one of the VCSEL TE polarised modes and the in-plane TE polarised mode. The other VCSEL TE polarised mode will also be identical for an in-plane symmetric active medium, and the modal gain will be related by differences in the confinement factor of each mode. Therefore, by calculating the respective confinement factors, the vertical-cavity material gain can be determined from measurements of the in-plane modal gain. The stripe-length method, also known as the

segmented-contact method, utilises a non-lasing test structure, to allow measurement of single-pass modal gain and prevent carrier pinning effects. Consequently, for the VCSEL structures it is necessary to also prevent lasing in the vertical direction and in what follows we describe a simple approach to ensure this. The threshold material gain can be determined by evaluating the material gain at the threshold current density and at the vertical-cavity resonance wavelength. The threshold current density can be found from optical power-current (P-I) characterisation of large oxide aperture VCSEL devices, and the resonance wavelength from surface photovoltage spectroscopy (SPVS).

2. Method

2.1. Experimental setup

Two nominally identical VCSEL epitaxial structures were grown for this study. Each sample consists of a one-wavelength thick cavity containing three 6 nm $In_{0.06}Ga_{0.94}As$ QWs with a graded AlGaAs SCH. The cavity was sandwiched between an upper p-doped and lower n-doped $Al_{0.12}Ga_{0.88}As/Al_{0.9}Ga_{0.1}As$ DBR mirror with graded interfaces. One sample had a 62 nm 'in-phase' cap layer and was grown by metal organic vapour-phase epitaxy (MOVPE), whilst the other sample had a 124 nm 'anti-phase' cap layer and was grown by molecular beam epitaxy. Both samples were grown on a GaAs substrate. The anti-phase top mirror layer increases the mirror loss, increasing the required threshold gain for lasing. In conjunction with an inverted surface relief, it is used to introduce a mode dependent mirror loss so that robust single-mode VCSEL devices can be fabricated [21, 22]. Such structures can also be advantageous for minimising round trip amplification (and therefore lasing) in the vertical direction while gain measurements are performed in the horizontal direction.

A schematic diagram of the segmented-contact device is shown in figure 1. Segmented Cr-Au contact pads, 292 μm long and 100 μm wide with 8 μm gaps, were patterned and annealed onto the p-GaAs cap surface and a planar, standard AuGe-Ni-Au contact deposited on the n-side, followed by a second annealing step. To increase the electrical resistance between each section, the p-GaAs cap layer and a small portion of the top p-DBR mirror pairs in the gap between contacts were wet etched away using the p-contact metal as the mask.

Figure 2 shows the dependence of the top mirror reflectivity (calculated using the transfer matrix method [23]) on the cap thickness due to the changes in the phase of the reflected light. In air, the 62 nm cap thickness device is aligned to the anti-phase reflectivity minimum, while the 124 nm cap thickness device is at an in-phase reflectivity maximum. Unlike a standard VCSEL structure the segmented contact structures require a metal contact that covers the top cap. With the addition of metal, due to the complex refractive index, the minimum shifts [24] and occurs at a cap thickness of approximately 93 nm, with neither cap thickness aligned to the anti-phase reflectivity minimum. Previous work [25–27] has indicated that this simple picture is altered: diffusion of Cr into GaAs

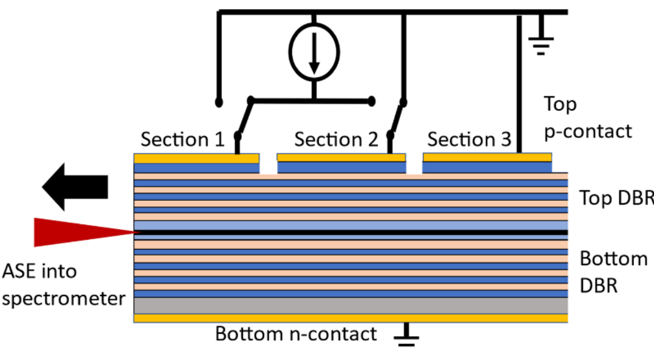

Figure 1. Schematic diagram of segmented contact devices.

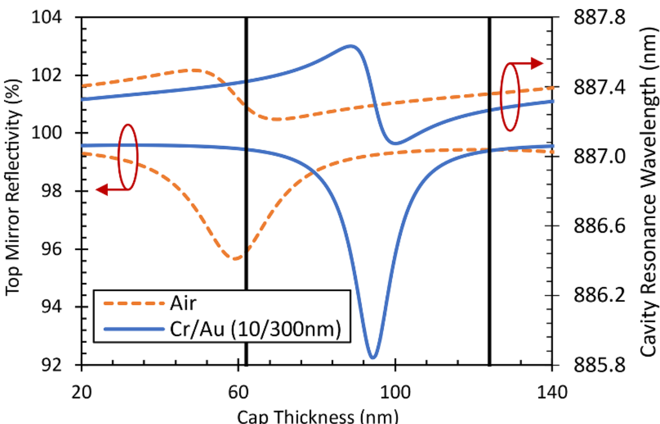

Figure 2. Top mirror reflectivity (left axis) and the respective cavity resonance wavelength (right axis) for varying cap thicknesses for air above the cap layer (dashed orange) and for Cr-Au layers deposited on top of the cap layer (solid blue). The vertical black lines denote the nominal cap thicknesses of the two samples.

upon deposition, and the expulsion of Ga and As from the intermixed Cr-GaAs interface following annealing, leads to an effective reduction in the p-GaAs cap optical thickness, changing the in-phase and anti-phase condition. We note that this effect is unlikely to align the effective cap thickness, of the initially 124 nm thick cap, to the anti-phase cap thickness. However, it will increase the top mirror loss sufficiently that the optical gain can be characterised at current densities close to the threshold current density. This combined with the results presented later in the paper lead us to label the samples with a 62 nm cap thickness as in-phase and the 124 nm cap thickness as anti-phase.

P-I curves were obtained for the in-plane and vertical emission of both the anti-phase and in-phase segmented-contact devices. For the vertical emission, some light emitted from regions below the contacts could be seen at the edge of the contacts and measured with an integrating sphere. To eliminate self-heating, the sections were pumped with an in-house pulsed current source, with a 1 kHz repetition frequency and a 1 μs pulse width, the same conditions as the gain measurements. To account for current spreading in the highly doped mirror layers, a factor of 0.73 $\pm$ 0.02 was applied to the current density determined from the contact area. Figure 3(a)

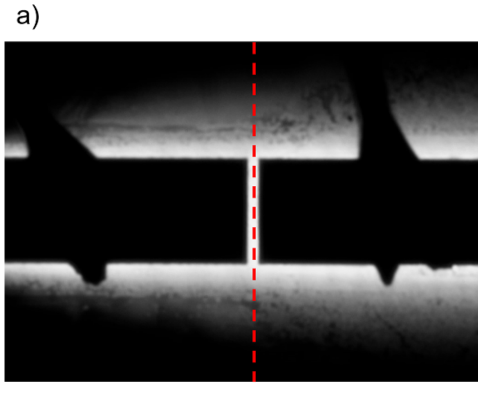

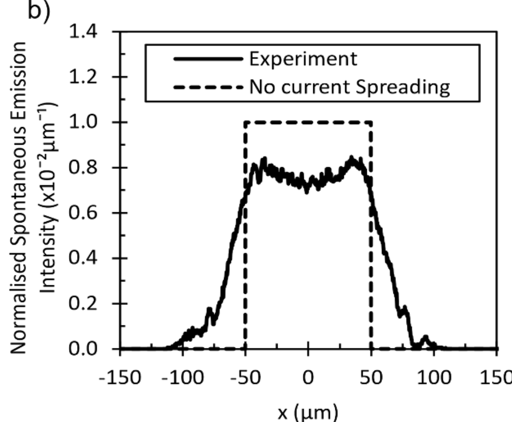

Figure 3. (a) Image showing the vertical emission from the top surface of a segmented contact device pumped at a current density of 0.29 kA cm^{-2}, and (b) the normalised measured intensity of the vertical emission (solid black), from the gap separating sections 1 and 2 (shown by the red dashed line in (a)), and the normalised intensity if no current spreading was present (dashed black) and the pumped area was equal to the contact area.

shows the vertical nearfield profile of the segmented contact device, with sections 1 and 2 pumped, and was imaged using a microscope objective lens, The current spreading factor was estimated from figure 3(b), which shows a line profile of the vertical spontaneous emission profile from the gap between sections 1 and 2. Assuming the intensity is linearly proportional to the current density, when compared to a profile assuming no current spreading is present, the current density in a 20 μm wide central portion is lower by 27%.

The in-plane amplified spontaneous emission (ASE) spectra from electrically pumping two adjacent sections, individually and then simultaneously, was measured. By pumping different number of sections, the pumped stripe length was altered, and the net modal gain $G-\alpha_i$ was calculated using equation (1) [20]

$$G-\alpha_i=\frac{1}{L}\ln\left(\frac{I_{\text{meas}}\,(1+2)}{I_{\text{meas}}\,(1)}-1\right) \tag{1}$$

where G is the per unit length modal gain generated in the QW layers, α_i is the internal optical mode loss which are any optical losses not due to absorption in the active region (this includes but is not limited to radiation losses, scattering by irregularities at interfaces, and absorption by free carriers), L is the length of a single segmented contact section, and $I_{\text{meas}}\,(\ldots)$ is the measured ASE with the pumped section denoted within the brackets. Equation (1) assumes that the ASE from only a single mode is measured.

The internal optical mode loss was determined by taking the mean value of the plateau region, where the gain spectra for different pumping level converge at wavelengths beyond the band edge. We assume here the internal optical mode loss is approximately constant over the wavelength range from the gain-peak wavelength to the plateau region.

The segmented contact devices were epoxied onto a gold TO-header that was mounted on a copper mount with a proportional-integral-derivative (PID) controlled heater plate. A lens was used to image the nearfield of the in-plane mode onto the slits of the spectrometer. The intensity was measured using a charge-coupled device (CCD) camera with partial vertical binning, so only light from the central portion of the nearfield was used to obtain the gain spectra. An iris was placed in front of the lens which limited the full width collection angle to approximately 4°, which reduces the collection of partially amplified light [28]. This also reduces the collection of slow light modes, that are present due to the vertical cavity structure [29, 30], as they have high edge emission angles close to the vertical cavity resonance wavelength. A linear polariser was placed in front of the spectrometer such that only the TE polarised ASE was transmitted.

VCSEL devices, with a mesa diameter of 44 μm, were fabricated from the same wafer using a quick fabrication (QF) process [31], and the substrate lapped to ~150 μm to reduce self-heating. They were oxidised with a 15.5 ± 0.5 μm oxidation extent to form devices with a nominal oxide aperture diameter of 13 μm, large enough that the transverse confinement would be close to unity and the self-heating low. The threshold current density was determined from P-I curves taken with a semi-automatic wafer prober fitted with an integrating sphere, and an in-house pulsed low-current source with a 10 μs pulse width and 1 kHz repetition frequency. Due to the proximity of the oxide aperture to the QW layers, current spreading in the QF VCSEL devices were assumed to be negligible. However, due to the smaller dimensions of the oxide aperture compared to the segmented contact devices, current spreading may still have a non-negligible effect on the measured threshold current density, and thus the measured material gain evaluated at the threshold current density.

The resonance wavelength of the vertical cavity structure was determined from SPVS, where the photo-voltage induced by light incident on the surface of the wafer is measured [32–34]. A sharp peak in the photo-voltage is seen at the cavity resonance wavelength due to a higher photon density, within the vertical cavity, increasing the number of electron–hole pairs generated at the active region.

2.2. Relation between in-plane modal gain and material gain

The relation between the modal gain and material gain, and the effect of dispersion have been frequently discussed in the literature. For longitudinally invariant waveguides, expressions have been derived that relate the material gain with the modal gain, which have shown the effective index can modify the modal gain [23, 35]. More recently, there has been interest in the gain in photonic crystals, which offer greater control of the dispersion, and a significantly reduced group velocity. Measurements performed on photonic crystal structures indicate a gain enhancement due to the reduced group velocity [36]. It was also reported in [37], that material dispersion does not appear to enhance the Beer–Lambert absorption.

For a dielectric waveguide, where the mode propagates along the z-direction, a general expression that relates the per-unit-length modal gain with the per-unit-length material gain, g was derived in [38]

$$G = \frac{\varepsilon_0 c n_{\mathrm{qw}} g \iint_{\mathrm{qw}} \left|\vec{E}\right|^2 dxdy}{\iint_{\mathrm{mode}} Re\left(\vec{E}\times\vec{H}^*\right)\cdot\hat{z}dxdy} \tag{2}$$

where n_{qw} is the refractive index of the QW layers, ε_0 is the permittivity of free space, c is the speed of light in a vacuum, $\vec{E}$ and $\vec{H}$ are the electric and magnetic field of the optical mode respectively. This equation is valid for both dispersive and non-dispersive material, and we find that material dispersion has no effect on the modal gain as in [37].

To describe the in-plane propagation of light, we treat the VCSEL structure as a multi-layer slab waveguide [23, 35], For the TE polarised mode, the real part of the Poynting vector along the direction of propagation evaluates to [35]

$$Re\left(\vec{E}\times\vec{H}^*\right)\cdot\hat{z} = n_{\mathrm{eff}} c\varepsilon_0 {E_0}^2 |U(y)|^2 \tag{3}$$

where n_{eff} is the effective of the mode, E_0 is the electric field amplitude, U is the TE field profile, and y is along the growth axis. Therefore, in agreement with [23] and [35], equation (2) for the TE polarised mode of a multi-layer slab waveguide simplifies to

$$G = \frac{n_{\mathrm{qw}}}{n_{\mathrm{eff}}}\Gamma g \tag{4}$$

where Γ is the confinement factor which describes the overlap of the electric field with the QW layers. The factor $n_{\mathrm{qw}}/n_{\mathrm{eff}}$ describes the increase in the effective interaction length of the mode with the QW layers due to light effectively bouncing up and down as it propagates along the waveguide [23]. Γ can be expressed as

$$\Gamma = \frac{\int_{\mathrm{qw}} |U(y)|^2 dy}{\int_{\mathrm{mode}} |U(y)|^2 dy} \tag{5}$$

We take the integral in the numerator over just the QW layers, and the integral in the denominator over the entire mode.

We assume that the gain is equally distributed across the quantum well layers, and that refractive index variations along the vertical axis have a negligible impact on the propagation of the vertical cavity mode in the QW layers. Additionally, we assume the lateral dimensions of the VCSEL device is large enough that the structure in the lateral direction can be taken to be uniform and the guiding by the oxide aperture is negligible. Therefore, the effective index of the vertical mode in the QW layers is approximately equal to the QW refractive index, so we can take the material gain determined from the in-plane modal gain to be the equal to the vertical material gain.

Strictly speaking, for light normally incident on a QW, the per unit length material gain is not a physically appropriate quantity [39]. When the quantum well width is varied, the amplification of light does not simply follow the Beer–Lambert Law. It is therefore more appropriate to use a fractional gain per well $\gamma_0 = gL_0$ [28, 39], where L_0 is the thickness of a single well. On the other hand, for the purposes of computational modelling, it is often more convenient to work with a material gain, and for the remainder of this work, we shall continue to use a material gain for the vertical direction.

With the above assumptions, the material threshold gain required for a VCSEL to lase can be calculated from [28]

$$\Gamma_{\mathrm{enh}} g L_{\mathrm{qw}} = \ln\left(\frac{1}{\sqrt{R_{\mathrm{top}} R_{\mathrm{bottom}}}}\right) \tag{6}$$

where Γ_{enh} is the gain enhancement factor due to standing wave effects, L_{qw} is the total thickness of the QW layers, and R_{top} and R_{bottom} are the reflectivity of the top and bottom layers respectively. Internal optical losses are included implicitly in R_{top} and R_{bottom}.

3. Results

Room temperature vertical and in-plane P-I characteristics (figures 4(a) and (b) respectively) indicate vertical amplification and possibly lasing, above a current density of 0.4 kA cm^{-2}, occurring in segmented contact devices fabricated from the sample with the in-phase top mirror design. The corresponding in-plane P-I curve, of the in-plane emission, shows that the slope of the curve reduces above a current density of 0.4 kA cm^{-2}, suggesting that the carrier density is clamping in certain areas of the active region, again indicative of amplification and lasing in the vertical direction. However, this is not observed in the anti-phase device, with no apparent threshold in the vertical emission, nor clamping of the in-plane emission. Therefore, gain measurements are performed on the anti-phase device, as the gain vs current density relation will not be complicated by carrier pinning effects.

The measured TE in-plane modal gain at 30 °C is shown in figure 5, for a range of injected current densities. The figure shows that at a current density of 0.417 kA cm^{-2}, the peak net-modal-gain is measured to be 36 $\pm$ 2 cm^{-1} at a wavelength of 892.6 $\pm$ 0.4 nm. At 1.147 kA cm^{-2}, the peak net-modal-gain increases to 70 $\pm$ 1 cm^{-1} and blueshifts to 887.4 $\pm$ 0.1 nm. From the plateau region over the wavelength range of 922.5–927.5 nm, the internal optical mode loss is determined to be 8.1 $\pm$ 0.7 cm^{-1}. We note that this in-plane loss may be different to that experienced in the vertical direction due to optical

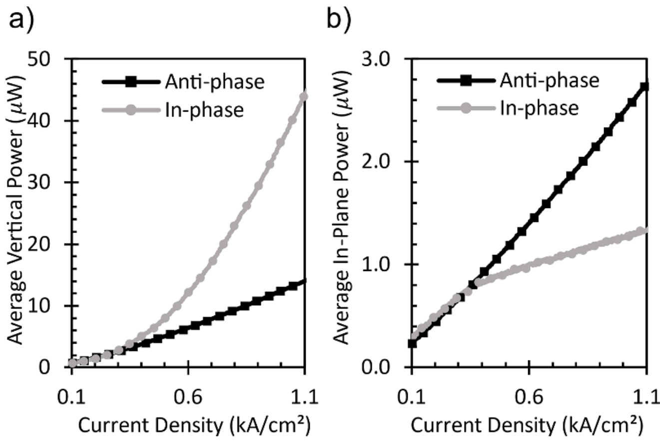

Figure 4. P-I curves of light emitted in the (a) vertical and (b) in-plane direction.

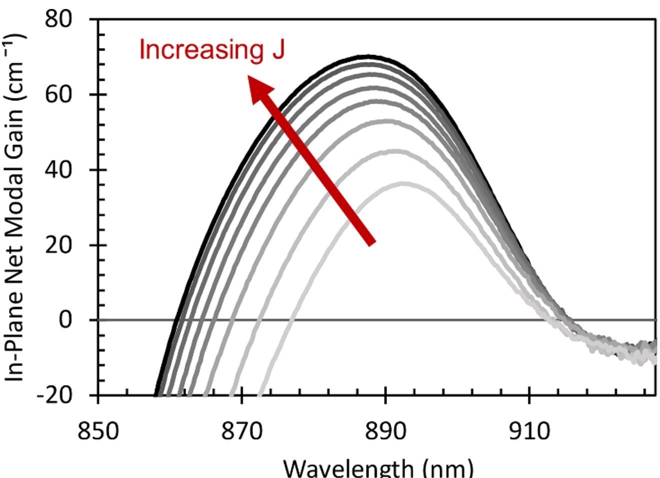

Figure 5. In-plane modal gain curves of the anti-phase device for a current density, J, range of 0.417–1.147 kA cm^{-2} in 0.104 kA cm^{-2} steps at a temperature of 30 °C.

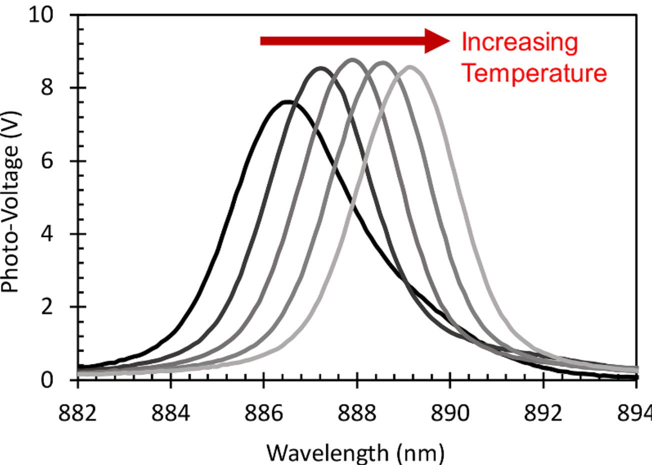

Figure 6. Photo-voltage spectra at temperatures of 30 °C–70 °C in 10 °C steps. The cavity resonance wavelength was determined from the peak position.

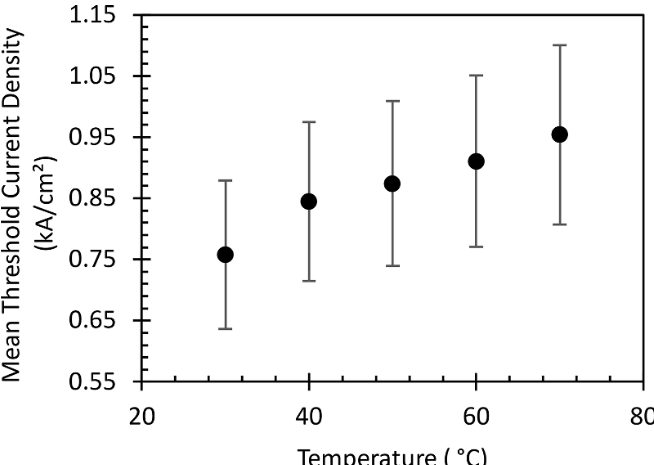

Figure 7. Mean threshold current density of the QF VCSEL devices at different substrate temperatures under pulsed operation.

scattering but is important here as it must be used to correct the net-modal-gain data to modal-gain, before calculating the material and VCSEL modal gain.

Figure 6 shows the photo-voltage spectra obtained using SPVS (as described in section 2.1). From the peak in the photo-voltage response, the cavity resonance wavelength is measured to be 886.5 ± 0.1 nm at 30 °C and redshifts to 889.1 ± 0.1 nm at 70 °C, giving a thermal tuning coefficient of 0.066 nm K^{-1} for the cavity resonance wavelength. There is an additional uncertainty due to variation in the cavity resonance wavelength of approximately ±2 nm across the 4″ wafer and the difference in location of the SPVS and segmented contact samples. Figure 7 shows the mean threshold current density of fabricated VCSEL devices at different temperatures which indicates the threshold current density minima occurs below 30 °C. This is consistent with the optical gain and cavity resonance measurements shown in figures 5 and 6, which shows the gain peak wavelength at a longer wavelength than the cavity resonance wavelength, even for a current density of 1.147 kA cm^{-2} which is above the measured threshold current density. Due to the higher thermal redshift of the gain-peak wavelength, this would indicate alignment of the gain-peak with the cavity resonance occurring at temperatures below 30 °C.

4. Discussion

The experimentally obtained in-plane modal gain at threshold was converted into a material gain using equations (4) and (5). Both the in-plane and vertical mode was calculated using the transfer matrix method outlined in [23] using refractive index values from [40–42], and [43]. Due to a lack of temperature dependent refractive index data for InGaAs above the bandgap energy, the bandgap energy value at room temperature was used, incurring an error of ∼10%, for the converted material gain, for a 1% change in the InGaAs refractive index value, due to changes in the confinement factor of the in-plane mode. Internal optical losses in the doped AlGaAs DBR layers (with C and Si as the acceptor and donor respectively) were included by adding an imaginary term to

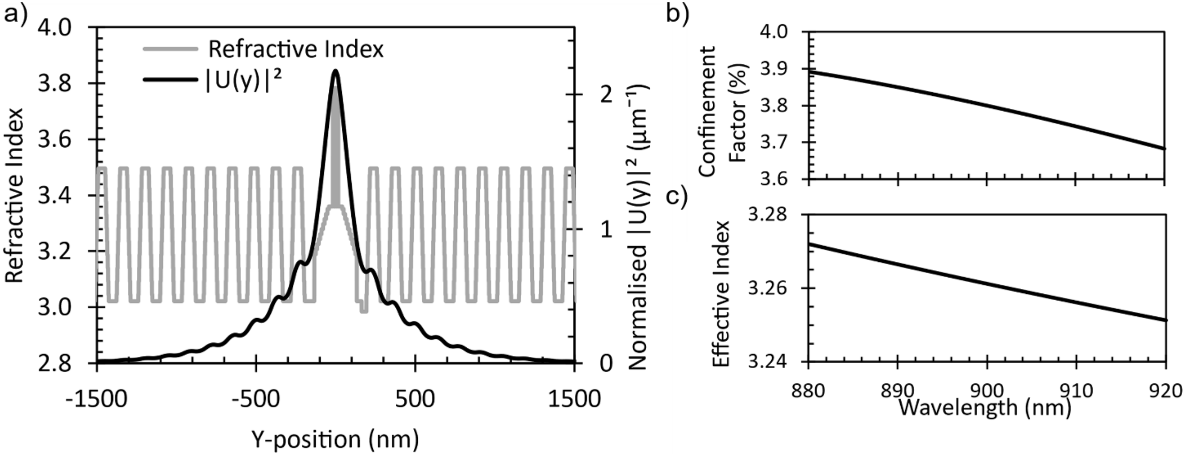

Figure 8. (a) Section of the refractive index profile (solid grey) and the calculated mode profile $|U(y)|^2$ (solid black) of the in-plane TE mode at the measured cavity resonance wavelength of 886.5 nm at 30 °C. Also shown is the calculated (b) confinement factor Γ, which gives the total coupling of the mode to all three wells, and (c) effective index n_{eff} over a wavelength range of 880–920 nm.

the refractive index values according to the doping concentration. Due to a lack of doping-induced absorption data for AlGaAs, absorption values for doped GaAs from [12] and [44] were used. In n-GaAs, the doping-induced absorption shows a weak wavelength dependence, and values at 1000 nm were used [12]. On the other hand, the absorption in p-GaAs (with Zn as the acceptor) is shown to have a λ^3 dependence [12], so the absorption values were extrapolated to 890 nm. Since C was the acceptor used for our structures, the absorption values used were double those for p-GaAs with a Zn acceptor [44].

Figure 8(a) shows the squared magnitude of the TE field profile of the fundamental TE-polarised mode, and the corresponding refractive index profile, at 886.5 nm at 30 °C. Figures 8(b) and (c) shows the calculated confinement factor and effective index respectively, over a wavelength range of 880–910 nm. Simulations indicate that, for the VCSEL structure considered here, a single index-guided TE polarised mode is present over the wavelength and temperature range of interest and suggests that our assumptions that the ASE from only a single mode is collected and that the internal optical loss is approximately constant is likely to be valid. On the other hand, for VCSEL structures where the in-plane mode is gain guided, the confinement factor will vary with the gain and the assumption that internal optical losses are constant may not be valid [45], in which case, further simulations would be necessary to correctly interpret the results.

Figure 9 compares the lasing threshold material gain calculated from the experimentally obtained in-plane modal gain (evaluated at the cavity resonance wavelength at the relevant temperature and at the current densities corresponding to threshold in the VCSEL) with the lasing threshold material gain determined using equation (6). Values of $n_{\mathrm{qw}} = 3.783$, $n_{\mathrm{eff}} = 3.268$ and $\Gamma = 0.0387$, evaluated at 886.5 nm, were used to convert the gain measured at 30 °C. The combined effect of these values on the converted material gain varied by ∼5% over the temperature range of interest. To determine the lasing threshold material gain for the vertical cavity resonance mode, values of $\Gamma_{\mathrm{enh}} = 1.86$, $R_{\mathrm{top}} = 99.42\%$, and $R_{\mathrm{bottom}} = 99.91\%$ were used at 30 °C.

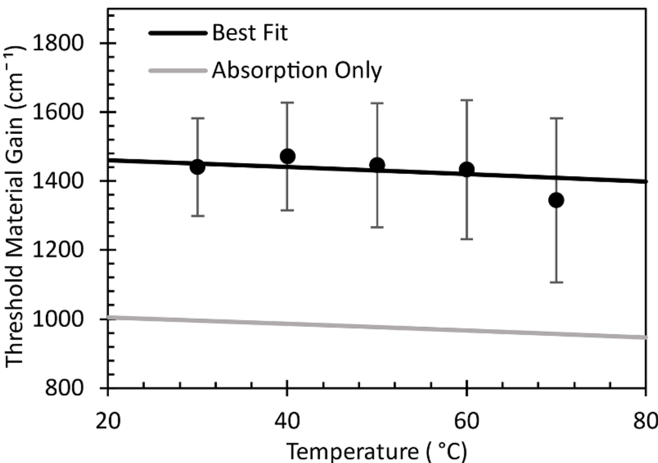

Figure 9. The lasing threshold gain calculated using equation (4) (solid lines) for the in-phase VCSEL device, and the experimentally obtained material gain at the lasing wavelength and threshold current density (black circles).

A measured threshold gain value of 1440 ± 140 cm^{-1} was obtained at 30 °C, with the uncertainty in the threshold gain values dominated by the uncertainty in the threshold current density due to the oxide aperture diameter. The plot indicates that when internal optical losses due to doping-induced absorption only are considered in equation (4), the calculated threshold material gain is underestimated by around ∼450 cm^{-1}. Additional scattering losses due to interface roughening in the n-DBR layers have been reported in [46]. Here a best fit is obtained when the optical loss in the n-DBR layers is increased from 7 cm^{-1} to 40 cm^{-1}. We deduce it is of the same order as the estimate of the optical loss of 80 ± 20 cm^{-1} obtained by linear interpolation of the values in [46], for a MOVPE grown n-DBR with the same nominal doping concentration of 2 × 10^{18} cm^{-3}. However, we note that a direct comparison is difficult due to differences in the material composition, growth method, and the operating wavelength. We also note that we have neglected other

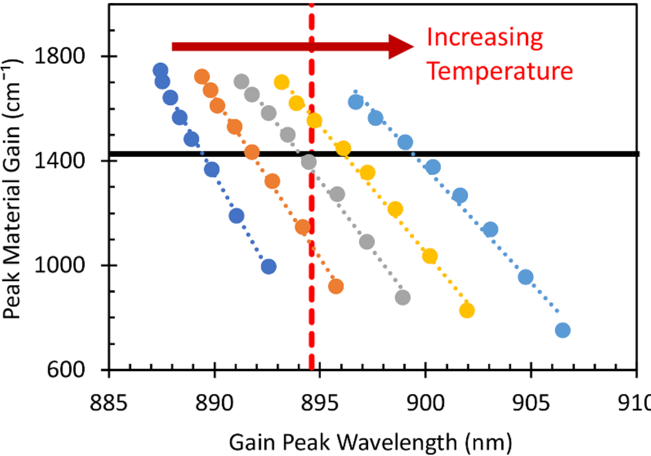

Figure 10. Experimentally obtained peak material gain values and the corresponding wavelength, with linear fits, at temperatures ranging from 30 °C to 70°C in 10 °C steps. The horizontal solid dark line indicates the experimentally obtained threshold material gain value at 30 °C. The vertical dashed red line shows the target operating wavelength of 894.6 nm.

possible loss mechanisms in our analysis, such as increased absorption in the SCH at high current injection [12].

Figure 10 shows the measured peak material gain and wavelength plotted for different current densities at different temperatures. The dashed red line shows the target lasing wavelength, and the solid black line shows the mean measured threshold material gain of 1430 ± 20 cm^{-1}. Where the lines cross correspond to the operating point of the intended VCSEL structure. Depending on the oxide aperture dimension, a typical device operating under continuous wave (CW) conditions might be expected to have an active region temperature approximately 20 °C higher than the substrate. The gain peak aligns with the targeted emission wavelength of 894.6 nm at a temperature of approximately 55 °C, indicating that for the current active region, the ideal CW operating temperature is 35 °C. However, for uncooled packaging, the VCSEL will likely operate at a higher operating temperature of 50 °C, depending on the application and environment. To illustrate the value of the gain measurements to the designer, we consider this scenario of wanting to operate at 50 °C, which would translate to an active region temperature of 70 °C. To satisfy the requirement, the 70 °C material gain peak value-wavelength line would need to be translated by approximately 5 nm to ensure it crosses the operating point. Such a relatively simple change could be implemented in subsequent growths by calibrating to a 5 nm blue shift in the room temperature active region photoluminescence (PL) peak.

5. Conclusion

The segmented-contact method has been demonstrated on VCSEL material. The measured gain peak to lasing wavelength detuning agrees well with the measured threshold current density temperature dependence, with the experimentally determined gain-peak to lasing-wavelength detuning and threshold current density minimum both occurring below 30 °C. The measured in-plane modal gain was converted to a material gain, giving a mean threshold material gain value of 1430 ± 20 cm^{-1}. This value indicates the presence of a loss mechanism in addition to the doping induced absorption, and agreement is found by increasing the optical loss in the n-DBR layers from 7 cm^{-1} to 40 cm^{-1}. This is consistent with previous work with additional scattering losses due to interface roughening in the n-DBR layers. To further demonstrate the utility of this technique, the experimentally determined peak material gain is plotted as a function of gain-peak wavelength, and it is shown that a 5 nm blueshift in the active region PL peak would optimize the active structure for CW operation at an ambient temperature of 50 °C. We envisage this technique could better inform the optimization process, reducing the development time and cost required to manufacture VCSEL devices with low threshold current and high yields.

Data availability statement

The data that support the findings of this study is available in the Cardiff University Research Data Archive and details on how to access it can be found at http://doi.org/10.17035/d.2022.0138005445.

Acknowledgments

Curtis Hentschel would like to thank Peter Blood for helpful discussions. The EPSRC funded Future Compound Semiconductor Manufacturing Hub: reference EP/P006973/1, the EPSRC funded CS Underpinning Equipment Grant: reference EP/P030556/1, and the Innovate UK funded CSconnected Strength in Places Fund (SIPF): reference 107134, provided essential resources for this study. Curtis Hentschel and Jack Baker would like to acknowledge support from an EPSRC Industrial-CASE award co-funded by IQE, Grant Nos. EP/S513611/1 and EP/T517525/1.

ORCID iDs

C Hentschel https://orcid.org/0000-0001-5420-8403
C P Allford https://orcid.org/0000-0002-3798-9014
S-J Gillgrass https://orcid.org/0000-0003-2611-9168
J Baker https://orcid.org/0000-0003-1379-0673
S Shutts https://orcid.org/0000-0001-6751-7790

References

[1] Iga K 2018 Forty years of vertical-cavity surface-emitting laser: invention and innovation *Jpn. J. Appl. Phys.* **57** 08PA01
[2] Liu A, Wolf P, Lott J A and Bimberg D 2019 Vertical-cavity surface-emitting lasers for data communication and sensing *Photon. Res.* **7** 121
[3] Khan Z, Shih J-C, Chao R-L, Tsai T-L, Wang H-C, Fan G-W, Lin Y-C and Shi J-W 2020 High-brightness and high-speed vertical-cavity surface-emitting laser arrays *Optica* **7** 267

[4] Serkland D K, Geib K M, Peake G M, Lutwak R, Rashed A, Varghese M, Tepolt G and Prouty M 2007 VCSELs for atomic sensors *Proc. SPIE* **6484** 648406

[5] Al-Samaneh A 2014 *PhD Thesis* Ulm University (https://doi.org/10.18725/OPARU-3205)

[6] Kitching J 2018 Chip-scale atomic devices *Appl. Phys. Rev.* **5** 031302

[7] Zhang J, Zhang X, Zhu H, Zhang J, Ning Y, Qin L and Wang L 2015 High-temperature operating 894.6nm-VCSELs with extremely low threshold for Cs-based chip scale atomic clocks *Opt. Express* **23** 14763

[8] Hakki B W and Paoli T L 1975 Gain spectra in GaAs double−heterostructure injection lasers *J. Appl. Phys.* **46** 1299

[9] Lu T-C, Chu J-T, Chen S-W, Cheng B-S, Kuo H-C and Wang S-C 2008 Lasing behavior, gain property, and strong coupling effects in GaN-based vertical-cavity surface-emitting lasers *Jpn. J. Appl. Phys.* **47** 6655

[10] Kuksenkov D V, Temkin H and Swirhun S 1995 Measurement of internal quantum efficiency and losses in vertical cavity surface emitting lasers *Appl. Phys. Lett.* **66** 1720

[11] Thibeault B J, Strand T A, Wipiejewski T, Peters M G, Young D B, Corzine S W, Coldren L A and Scott J W 1995 Evaluating the effects of optical and carrier losses in etched-post vertical cavity lasers *J. Appl. Phys.* **78** 5871

[12] Babic D I, Piprek J, Streubel K, Mirin R P, Margalit N M, Mars D E, Bowers J E and Hu E L 1997 Design and analysis of double-fused 1.55-μm vertical-cavity lasers *IEEE J. Quantum Electron.* **33** 1369

[13] Hofmann M R *et al* 2002 Emission dynamics and optical gain of 1.3-μm (GaIn)(NAs)/GaAs lasers *IEEE J. Quantum Electron.* **38** 213

[14] Ikyo A B, Marko I P, Hild K, Adams A R, Arafin S, Amann M-C and Sweeney S J 2016 Temperature stable mid-infrared GaInAsSb/GaSb vertical cavity surface emitting lasers (VCSELs) *Sci. Rep.* **6** 19595

[15] Soda H, Motegi Y and Iga K 1983 GalnAsP/InP surface emitting injection lasers with short cavity length *IEEE J. Quantum Electron.* **19** 1035

[16] Ledentsov N N, Shchukin V A, Kalosha V P, Ledentsov N N, Kropp J-R, Agustin M, Chorchos Ł, Stępniak G, Turkiewicz J P and Shi J-W 2018 Anti–waveguiding vertical–cavity surface–emitting laser at 850 nm: from concept to advances in high–speed data *Opt. Express* **26** 445

[17] Geels R S, Corzine S W and Coldren L A 1991 InGaAs vertical-cavity surface-emitting lasers *IEEE J. Quantum Electron.* **27** 1359

[18] Kajita M, Kawakami T, Nido M, Kimura A, Yoshikawa T, Kurihara K, Sugimoto Y and Kasahara K 1995 Temperature characteristics of a vertical-cavity surface-emitting laser with a broad-gain bandwidth *IEEE J. Sel. Top. Quantum Electron.* **1** 654

[19] Ghosh S, Constant S, Hosea T J C and Sale T E 2000 Edge-emission electroluminescence study of as-grown vertical-cavity surface-emitting laser structures *J. Appl. Phys.* **88** 1432

[20] Blood P, Lewis G M, Smowton P M, Summers H, Thomson J and Lutti J 2003 Characterization of semiconductor laser gain media by the segmented contact method *IEEE J. Sel. Top. Quantum Electron.* **9** 1275

[21] Unold H J, Mahmoud S W Z, Jäger R, Grabherr M, Michalzik R and Ebeling K J 2001 Large-area single-mode VCSELs and the self-aligned surface relief *IEEE J. Sel. Top. Quantum Electron.* **7** 386

[22] Haglund Å, Gustavsson J S, Vukušić J, Modh P and Larsson A 2004 Single fundamental-mode output power exceeding 6 mW from VCSELs with a shallow surface relief *IEEE Photonics Technol. Lett.* **16** 368

[23] Coldren L A, Corzine S W and Mašanović M L 2012 *Diode Lasers and Photonic Integrated Circuits* (Hoboken, NJ: Wiley)

[24] Smolyakov G A and Osiński M 2005 Analysis of lateral-mode confinement in VCSELs with ring metal apertures *J. Lightwave Technol.* **23** 4278

[25] Weaver J H, Grioni M and Joyce J 1985 Critical development stages for the reactive Cr-GaAs(110) interface *Phys. Rev.* B **31** 5348

[26] Xu F, Lin Z, Hill D M and Weaver J H 1987 Temperature-dependent interface evolution for Ti/GaAs(100) and Cr/GaAs(100) *Phys. Rev.* B **36** 6624

[27] Hill D M, Xu F, Lin Z and Weaver J H 1988 Atomic distributions across metal–III-V-compound-semiconductor interfaces *Phys. Rev.* B **38** 1893

[28] Blood P 2015 *Quantum Confined Laser Devices: Optical Gain and Recombination in Semiconductors* (Oxford: Oxford University Press)

[29] Gu X, Shimada T and Koyama F 2011 Giant and high-resolution beam steering using slow-light waveguide amplifier *Opt. Express* **19** 22675

[30] Hayakawa J, Murakami A, Tominaga D, Suzuki Y, Ho Z, Gu X and Koyama F 2019 Watt-class high-power and high beam-quality VCSEL amplifiers *Proc. SPIE* **10938** 1093809

[31] Baker J, Gillgrass S-J, Allford C P, Peach T, Hentschel C, Sweet T, Davies J I, Shutts S and Smowton P M 2022 VCSEL quick fabrication for assessment of large diameter epitaxial wafers *IEEE Photonics J.* **14** 1530110

[32] Ashkenasy N, Leibovitch M, Rosenwaks Y and Shapira Y 2000 Characterization of quantum well structures using surface photovoltage spectroscopy *Mater. Sci. Eng.* B **74** 125

[33] Liang J S, Huang Y S, Tien C W, Chang Y M, Chen C W, Li N Y, Li P W and Pollak F H 2001 Surface photovoltage spectroscopy characterization of a GaAs/GaAlAs vertical-cavity-surface-emitting-laser structure: angle dependence *Appl. Phys. Lett.* **79** 3227

[34] Huang Y S, Malikova L, Pollak F H, Debray J-P, Hoffman R, Amtout A and Stall R A 2002 Surface photovoltage spectroscopy and normal-incidence reflectivity characterization of a 1.3 μm InGaAlAs/InP vertical-cavity surface-emitting laser structure *J. Appl. Phys.* **91** 6203

[35] Visser T D, Blok H, Demeulenaere B and Lenstra D 1997 Confinement factors and gain in optical amplifiers *IEEE J. Quantum Electron.* **33** 1763

[36] Ek S, Lunnemann P, Chen Y, Semenova E, Yvind K and Mørk J 2014 Slow-light-enhanced gain in active photonic crystal waveguides *Nat. Commun.* **5** 5039

[37] Thevenaz L, Chin S, Dicaire I, Beugnot J-C, Mafang S F and Herráez M G 2009 Experimental verification of the effect of slow light on molecular absorption *Proc. SPIE* **7503** 75034W

[38] Ning C Z 2010 Semiconductor nanolasers *Phys. Status Solidi* b **247** 774

[39] Blood P 2000 On the dimensionality of optical absorption, gain, and recombination in quantum-confined structures *IEEE J. Quantum Electron.* **36** 354

[40] Alam M S, Rahman M S, Islam M R, Bhuiyan A G and Yamada M 2007 Refractive index, absorption coefficient, and photoelastic constant: key parameters of InGaAs material relevant to InGaAs-based device performance *2007 IEEE 19th Int. Conf. on Indium Phosphide & Related Materials* p 343

[41] Gehrsitz S, Reinhart F K, Gourgon C, Herres N, Vonlanthen A and Sigg H 2000 The refractive index of $Al_xGa_{1-x}As$ below the band gap: accurate determination and empirical modeling *J. Appl. Phys.* **87** 7825
[42] Johnson P B and Christy R W 1974 Optical constants of transition metals: Ti, V, Cr, Mn, Fe, Co, Ni, and Pd *Phys. Rev.* B **9** 5056
[43] Johnson P B and Christy R W 1972 Optical constants of the noble metals *Phys. Rev.* B **6** 4370
[44] Kiyota K, Kageyama T, Shimizu H and Kawakita Y 2009 Measurement of absorption coefficient of carbon-doped GaAs *Jpn. J. Appl. Phys.* **48** 111103
[45] Siegman A E 2003 Propagating modes in gain-guided optical fibers *J. Opt. Soc. Am.* A **20** 1617
[46] Asplund C, Mogg S, Plaine G, Salomonsson F and Chitica N 2001 Doping-induced losses in AlAs/GaAs distributed Bragg reflectors *J. Appl. Phys.* **90** 794